Pergamon

Int. J. Heat Mass Transfer. Vol. 40, No. 15, pp. 3663–3673, 1997

Printed in Great Britain
0017–9310/97 $17.00+0.00

PII: S0017–9310(96)00382–1

The influence of an advecting vortex on the heat transfer to a liquid droplet

M. MASOUDI and W. A. SIRIGNANO

Department of Mechanical and Aerospace Engineering, University of California, Irvine, Irvine, CA 92697, U.S.A.

(*Received* 21 *May* 1996 *and in final form* 9 *November* 1996)

Abstract—The unsteady three-dimensional interaction of an initially cylindrical vortex tube with a droplet in a uniform stream is investigated through a numerical solution of the Navier–Stokes equations. Particular attention is given to the effect of the vortex on the droplet convective heat transfer. The transient response of the droplet Nusselt number is sensitive to the geometrical factors that specify the vortex initial position and structure. The time-averaged Nusselt number is approximately the value for the axisymmetric case when the vortex center approaches the droplet along the base flow symmetry axis; otherwise, it varies monotonically with the vortex initial distance from the base flow symmetry axis, vortex circulation, and base flow Reynolds number. Beyond a certain range, the time-averaged Nusselt number reaches an asymptotic value. A correlation quantifying average effects of the vortex advection on the droplet heating, signifying a self-similar pattern in this unsteady problem, has been produced, and is shown to be also applicable to a rigid sphere in a comparable condition. This correlation compliments the existing ones for droplet heating in an axisymmetric flow. Based on these findings, it may be speculated that, in a spray combustion system, the vortex–droplet interactions within the Kolmogorov scale can have significant effects on the droplet convective heat transfer. © 1997 Elsevier Science Ltd.

1. INTRODUCTION

The fluid dynamics and heat transport for a cold liquid droplet in a hot gaseous axisymmetric environment is a well-understood phenomenon, and there exists substantial literature exploring many different aspects of such problems [1]. There is, however, a shortage of literature exploring droplet heating and vaporization when the far-field flow embracing the droplet undergoes temporal and/or spatial variations. The existing literature has focused on variations due to acoustical waves [2–4]. Vortical disturbances have not been widely examined.

Such a class of problems appears when the droplet transport properties are subject to velocity and temperature fluctuations in a turbulent flow, such as might occur in a liquid-fueled combustor. In particular, in a spray-droplet system, the droplet size is ~ 100 microns. In the turbulence spectrum for many continuous combustors, this length-scale corresponds to that of the Kolmogorov scale; thus, the droplet transport phenomena can be subject to turbulent effects primarily associated with those of the Kolmogorov scale. Moreover, since turbulence could be represented as a manifestation of vortex dynamics [5], it is useful to study the effect of an array of vortices on the droplet where the size of the vortices is comparable with that of the droplet. In the present work, the effect of one advecting vortex on a droplet was studied.

2. FLOW DESCRIPTION, GOVERNING EQUATIONS, AND VORTEX CHARACTERISTICS

The solution for the velocity field in this problem has been reported in previous publications [6, 7]. A summary of the present approach, including the governing equations, the boundary and initial conditions, the computational approach, and the reasons necessitating a parameter study, is presented below.

Consider a cold droplet impulsively injected in a hot gaseous environment with the droplet subsequently subjected to an unsteady interaction with an advecting vortex tube. The problem is non-linear by nature. Fundamental fluid dynamic aspects such as lift, drag, and moment coefficients of the vortex–droplet interaction were reported [6, 7], and thus, here, attention is given to recent findings on variations in the droplet heat transfer. Constant properties are assumed in both the gas and the liquid domain, and the droplet experiences no vaporization. The deceleration of the droplet due to the drag force is not considered.

Since the goal is to study the flow interaction with a liquid droplet, the governing equations for both the gas and the liquid phase are solved. These are the Navier–Stokes and thermal energy equations in both phases; the continuity equation is satisfied through pressure correction. The equations and boundary conditions are non-dimensionalized using the droplet radius a' as the characteristic length, the undisturbed

NOMENCLATURE

a' dimensional droplet radius (characteristic length)
d vortex offset distance from the base flow symmetry axis (normalized by a')
N_1, N_2, N_3 number of grid points in (ξ, η, ζ)
Nu Nusselt number
p pressure
Pr Prandtl number
q'' heat flux
r, θ, ϕ spherical coordinates
Re base flow Reynolds number (based on droplet diameter)
t time (normalized by a'/U'_∞)
T temperature
u, v, w flow velocities in (x, y, z) directions (normalized by U'_∞)
U'_∞ dimensional free-stream velocity (characteristic velocity)
v_{max} maximum tangential velocity of vortex tube (normalized by U'_∞)
V velocity vector
x, y, z Cartesian coordinates.

Greek symbols
Γ vortex tube circulation
(ξ, η, ζ) computational coordinates
σ radius of vortex tube (normalized by a')
ν' kinematic viscosity of the gas phase
τ shear stress
ψ stream function.

Superscript
$'$ dimensional quantity.

Subscripts
0 initial quantity
ax quantity in the corresponding axisymmetric flow (no vortex)
g quantity in the gas phase
l quantity in the liquid phase
s droplet surface (gas–liquid interface)
v vortex quantity.

free stream velocity U'_∞ as the characteristic velocity, and the ambient gas temperature T'_g as the characteristic temperature. The governing equations are:

Gas phase

$$\nabla \cdot V_g = 0 \tag{1}$$

$$\frac{DV_g}{Dt} = -\nabla p_g + \frac{2}{Re_g}\nabla^2 V_g \tag{2}$$

$$\frac{DT_g}{Dt} = \frac{2}{Re_g Pr_g}\nabla^2 T_g \tag{3}$$

Liquid phase

$$\nabla \cdot V_l = 0 \tag{4}$$

$$\frac{DV_l}{Dt} = -\nabla p_l + \frac{2}{Re_l}\nabla^2 V_l \tag{5}$$

$$\frac{DT_l}{Dt} = \frac{2}{Re_l Pr_l}\nabla^2 T_l. \tag{6}$$

These governing equations are transformed to the coordinates (ξ, η, ζ) (Fig. 1). ξ is the radial, η is the angular, and ζ is the azimuthal direction. The numerical integration of the equations is performed using a computational cubic mesh with equal spacing $(\delta\xi = \delta\eta = \delta\zeta = 1)$.

2.1. *Gas–liquid interface conditions*

The conditions at the interface are based on the principle of continuity of shear stresses (the discontinuity in shear stress across the surface due to surface tension gradient has been shown to be negligible in its impact on droplet heating), zero normal velocity, continuity of tangential velocities, continuity of the heat flux, and continuity of temperature. Since the interface is always spherical (under the assumption of small Weber number), these conditions are conveniently cast in terms of spherical coordinates (r, θ, ϕ) with the origin at the center of the droplet. This allows the interface conditions to be applied at a constant value of the radius; the axisymmetric base case is also more easily expressed. The (ξ, η, ζ) coordinates have the same orientation as the spherical coordinates (r, θ, ϕ), but obey an imposed stretching, allowing a relatively denser grid concentration near the gas–liquid interface (droplet surface):

$$\tau_{l,r\theta,s} = \tau_{g,r\theta,s}$$

$$\tau_{l,r\phi,s} = \tau_{g,r\phi,s}$$

$$V_{l,\theta,s} = V_{g,\theta,s}$$

$$V_{l,\phi,s} = V_{g,\phi,s}$$

$$T_{l,s} = T_{g,s}$$

$$q''_{l,s} = q''_{g,s}$$

where $\tau_{r\theta,s}$ and $\tau_{r\phi,s}$ are, respectively, the shear stresses on a positive r-plane in the positive θ- and ϕ-directions and q'' is the heat flux from the hot ambient gas into the cold liquid droplet. The interface condition for pressure is obtained from the momentum equation;

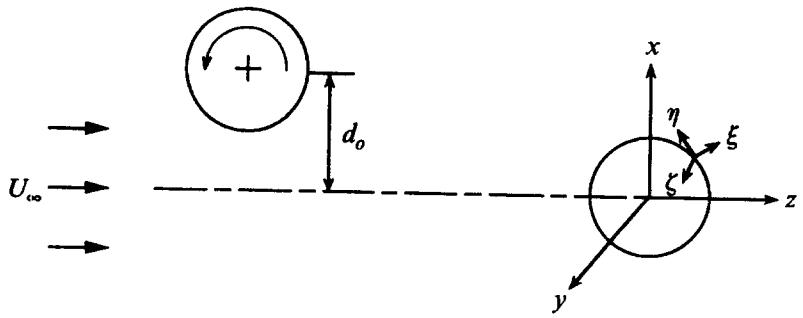

Fig. 1. Flow geometry and coordinates.

note that, for a spherical droplet, the pressure gradient is continuous across the interface.

2.2. *Gas-phase boundary conditions*

(N_1, N_2, N_3) and (N_{1l}, N_2, N_3) are the number of grid points in the gas and liquid domain, respectively, in (ξ, η, ζ) coordinates. ξ at N_{1l} and N_1 are the droplet surface and the gas far-field, respectively. The imposed far-field pressure, gas velocities in the (x, y, z) directions and gas temperature are

$$p = 0 \quad u = v = 0 \quad w = 1 \quad T = 1 \quad \text{at } \xi = N_1 \text{ and}$$

$$N_{2\text{mid}} \leqslant \eta \leqslant N_2 \text{ (upstream)}$$

$$p = 0 \quad \frac{\partial u}{\partial \xi} = \frac{\partial v}{\partial \xi} = \frac{\partial w}{\partial \xi} = \frac{\partial T}{\partial \xi} = 0 \quad \text{at } \xi = N_1 \text{ and}$$

$$1 \leqslant \eta < N_{2\text{mid}} \text{ (downstream)}.$$

The imposed initial conditions inside the liquid droplet are a quiescent liquid phase and a uniform temperature $T_{l0} < T_{g0}$.

2.3. *Symmetry conditions*

Since the cylindrical vortex tube advects with its axis of symmetry parallel to the y-axis, symmetry is maintained such that a solution is found for half the spherical domain rather than the entire domain, thus reducing the computational time:

$$\frac{\partial p}{\partial \zeta} = \frac{\partial u}{\partial \zeta} = \frac{\partial w}{\partial \zeta} = \frac{\partial T}{\partial \zeta} = 0 \quad v = 0 \quad \text{at } \zeta = 1, N_3.$$

2.4. *Numerical solution*

A three-dimensional implicit finite-difference algorithm solves the set of discretized partial differential equations. The control volume formulation is used to develop the finite-difference equations. The method of solution employs an alternating-direction-predictor–corrector (ADPC) scheme to solve the time-dependent equations.

The overall solution procedure is based on a cyclic series of estimate-and-correct operations. At each time-step, the solution in the gas phase is noticed first; the velocity components are first calculated from the momentum equations using the ADPC method, where the pressure field at the previous time-step is employed. This estimate improves as the overall iteration continues. The pressure is calculated from the pressure correction equation using the successive over-relaxation method. The new estimates of pressure and velocities are then obtained. These known quantities are used in the energy equation to solve for the gas-phase temperature field.

The interface conditions are next used to solve for the liquid-phase boundary values, followed by the sequential, iterative solution of the liquid-phase equations of motion and thermal energy until convergence is achieved for each time-step of the calculation.

At each time-step, the drag, lift, and moment coefficients and Nusselt number are evaluated. The entire procedure is then repeated for the next time-step. Further details may be found in previous publications of this research group [6–8]. High-precision computations for benchmarking purposes were executed on the Cray, taking an average runtime of about 10 cpu h. However, by using a normalization procedure (see end of Section 2.7), such long computations were avoided, and, using less mesh points, most executions were pursued on a Dec-alpha, Convex 240 or 3840, taking average runtimes of about 1.2, 1 or 0.9 cpu h, respectively.

2.5. *The vortex tube features*

The vortex is introduced upstream of the droplet, advects with the superimposed uniform flow, and has a relatively simple configuration—it is an initially cylindrical tube whose axis of symmetry is initially normal to the uniform flow and parallel to the y-axis. The vortex tube has a small central core; within this core, the initial velocity distribution in the vortex tube is that of solid body rotation reaching an imposed $v_{\max}$ at radius σ. $v_{\max}$ and σ are specified at time $t = 0$. Outside this inner core, the vortex induces a velocity

field of a potential vortex; thus, the velocity induced by the vortex vanishes as $r \to \infty$. This two-dimensional vortical tube is known as a Rankine vortex [9], and has the following stream function [10]:

$$\psi_v(x, z, t = 0) = -\frac{\Gamma_0}{2\pi} \ln [(x - x_0)^2 + (z - z_0)^2 + \sigma_0^2] \tag{7}$$

where Γ_0 is the initial non-dimensional vortex circulation at radius σ_0. Γ_0 is positive when the vortex tube has a counterclockwise rotation, and x_0 and z_0 denote the initial location of the center of the vortex tube. Note that the initial vortex tube circulation at radius σ_0 is $\Gamma_0 = 2\pi\sigma_0 v_{max0}$. After the initial time, the advection, diffusion and distortion (strain) on the vortex is determined through the solution of the Navier–Stokes equations. More fundamental information on the vortex tube, such as temporal changes in its tangential velocity and vorticity, are given in Ref. [6].

2.6. *Flow interaction*

The droplet is placed in a uniform flow (here also called the 'base flow'), and thus gradually develops a standing vortex ring in its aft position. Note that, in the absence of the vortex, the flow remains axisymmetric with respect to the z-axis (Fig. 1). The vortex is introduced 10 droplet radii upstream of the droplet and advects, initially, with the superimposed uniform free-stream flow and, later, with the local velocity; it takes about 10 residence time units for the vortex to arrive at the vicinity of the droplet; there, vortex stretching is observed in the cross-flow direction, and thus a full unsteady and three-dimensional interaction occurs between the vortex and the droplet. The dynamic interaction is the strongest when the vortex is initially introduced 'on' the base flow symmetry axis of Fig. 1; here, a 'head-on' collision between the droplet and the vortex is observed, resulting in a slow-down of the vortex advection, and also vortex stretching in the cross-flow direction. When the vortex advects 'off' the axis, the dynamic interaction between the two is relatively weaker and the vortex therefore advects nearly steadily with the base flow. It takes nearly 25 residence time units for the vortex to arrive at the droplet, interact with it, and then travel sufficiently far downstream to have insignificant influence. Many details of the interactions have been reported in Ref. [6].

2.7. *The droplet convective heat transfer*

The droplet convective heat transfer, represented by its Nusselt number, is computed through $Nu(t) = 2a'h'/k'_g$ (with h' and k'_g being the convective heat transfer coefficient and gas conductivity), which, after standard simplification and non-dimensionalization, yields

$$Nu(t) = \frac{\int_0^{\pi}\int_0^{\pi} \left.\frac{\partial T_g(t)}{\partial r}\right|_s \sin\theta \, d\theta \, d\phi}{\pi(1 - \overline{T_s})}$$

where $\overline{T_s}$ is the droplet temperature at the interface averaged over the surface. Since the cold droplet is injected impulsively in the hot ambient gas, it initially experiences a stronger heat transfer. In the base axisymmetric flow, it takes nearly five resident time units for the droplet Nusselt number to reach a steady value. However, when the vortex is superimposed on the base flow, the Nusselt number fluctuates continuously due to the advection of the vortex, and cannot attain a steady value. It is therefore more convenient to regard overall estimates by considering time-averaged and root-mean-squared values according to

$$\overline{Nu} = \frac{1}{t_2 - t_1} \int_{t_1}^{t_2} Nu(t) \, dt \tag{8}$$

and

$$Nu_{rms} = \sqrt{\overline{[Nu(t) - \overline{Nu}]^2}} = \sqrt{\frac{1}{t_2 - t_1} \int_{t_1}^{t_2} [Nu(t) - \overline{Nu}]^2 dt}. \tag{9}$$

It is advantageous to normalize $\overline{Nu}$ and Nu_{rms} using their corresponding values in an axisymmetric flow, $\overline{Nu}_{ax}$ and $Nu_{rms_{ax}}$; there is a substantial computational advantage to this normalization—while different values are obtained for $\overline{Nu}$ depending on the number of computational mesh points (ordinarily, 41 in each direction), the same values of $\overline{Nu}/\overline{Nu}_{ax}$ result in only half as many mesh points (21 in each direction) since both the numerator and the denominator change by the same amount, about 10%, due to a reduction in the number of mesh points. Therefore, $\overline{Nu}/\overline{Nu}_{ax}$ and $Nu_{rms}/Nu_{rms_{ax}}$ are considered in the present results. In the above estimates, $t_1 = 2$ and $t_2 = 25$, i.e. the data for $t \in (0,2)$ are disregarded; this is the time needed for the initial computational fluctuations in the pressure drag to vanish. To minimize the influence of this initial data exclusion on the final outcome, the normalizing values $\overline{Nu}_{ax}$ and $Nu_{rms_{ax}}$ are also estimated with this criterion imposed. Computed $\overline{Nu}/\overline{Nu}_{ax}$ are more invariant to this initial data exclusion than $Nu_{rms}/Nu_{rms_{ax}}$ are. (Sample comparisons show $\overline{Nu}/\overline{Nu}_{ax}$ and $Nu_{rms}/Nu_{rms_{ax}}$ values computed with and without this initial data exclusion vary by nearly or less than 0.05% and 8%, respectively.)

3. RESULTS

The velocity and thermal boundary layers, both in the gas phase and within the droplet interior, could be affected due to the advection of the vortex near the droplet. The vortex advection near the droplet breaks down the symmetry. In addition, the vortex could drastically change the structure of the recirculation zone in the droplet near wake, and cause its otherwise confined pockets of vorticity to be ejected into the free stream and to advect with the outer stream [6]. Further, due to the coupling between the velocity and temperature fields, all the developments in the velocity

boundary layer induced by the vortex advection have their corresponding effect on the thermal boundary layer as well. The substantial density ratio between the gas and liquid phases nevertheless makes the vortex effect more pronounced in the gas phase.

There are four parameters that characterize the quantitative significance of the vortex–droplet interaction: the vortex initial core size (σ_0), its initial maximum tangential velocity (v_{max0}), the offset distance between the vortex initial position and the base flow symmetry axis (d_0), and the base flow Reynolds number (Re). The initial position of the vortex center is placed 10 droplet radii upstream of the droplet, either 'on' the base flow symmetry axis ($d_0 = 0$) or slightly 'off' it ($d_0 = \pm 1, \pm 2, \ldots$). A positive or negative d_0 means an offset distance from the z-axis in the x, z symmetry plane in the positive or negative x-direction, respectively; this is shown in Fig. 1 with d_0 non-dimensionalized by the droplet radius.

An initial radius (σ_0) is specified for the vortex which defines the vortex core within which vorticity is uniformly distributed; the strength of this vorticity is chosen so that the maximum velocity at the core of the vortex (v_{max0}) represents an acceptable fluctuation from the uniform flow. This fluctuation is taken to be less than the free-stream velocity. For example, to represent a 20% fluctuation in the base flow, $v_{max0} = 0.2$ is chosen. Outside the inner core, the velocity pattern is that of a potential vortex. Thus, the vortex structure and strength are initially fully characterized by the two parameters σ_0 and v_{max0}, non-dimensionalized by the droplet radius and the strength of the uniform stream, respectively. Figure 1 shows a typical vortex location upstream of the droplet. Since, in the absence of the vortex, the base flow remains axisymmetric at all times, a change in the orientation of the vortex circulation only rotates the spatial orientation of the events; therefore, the counterclockwise orientation for the vortex is arbitrarily chosen in all of the simulations. A counterclockwise rotation with a positive offset distance is the mirror image of a clockwise rotation with a negative offset distance so that clockwise rotation need not be considered.

In order to investigate the droplet heat transfer influenced by the flow fluctuations due to the passage of the vortex, a parameter study is insured to determine the role of each of the four above characteristics on the droplet Nusselt number. The considered ranges are $d_0 = 0, \pm 1, \pm 2, \pm 3, \pm 4, \pm 5$; $\sigma_0 = 0.25, 0.5, 1, 2, 3, 4$; $v_{max0} = 0.1, 0.2, 0.3, 0.4$; and $20 \leqslant Re \leqslant 100$.

3.1. *The effect of the offset distance*

Figure 2(a) and (b) shows the temporal changes in the Nusselt number as a function of the vortex center initial position (d_0) upstream of the droplet. The droplet Nusselt number in an axisymmetric flow (i.e. having the same Reynolds number and without a vortex) is also shown for comparison. The substantial difference in the temporal response is apparent. The droplet Nusselt number increases for $d_0 > 0$, and decreases for

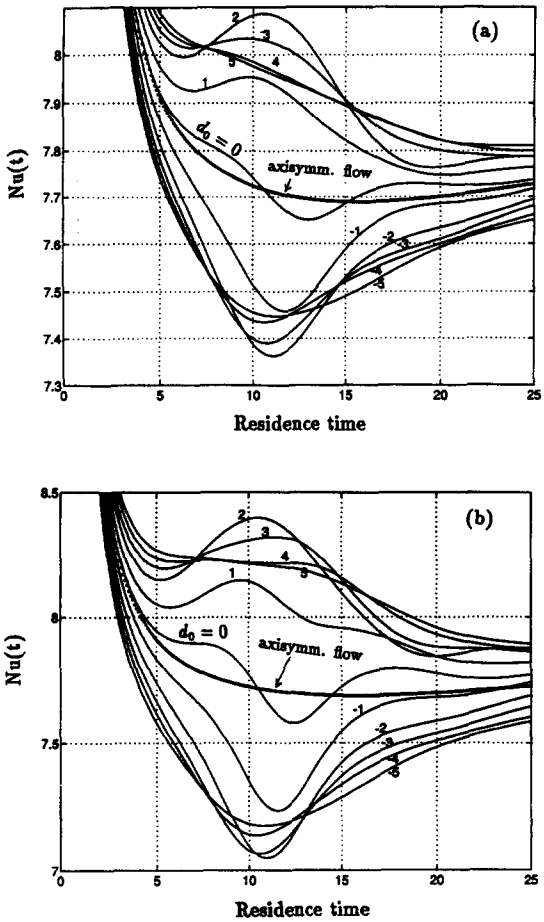

Fig. 2. Influence of the vortex initial offset distance (d_0) on $Nu(t)$: (a) vortex advecting with d_0 in $-5 \leqslant d_0 \leqslant 5$ ($\sigma_0 = 1$, $Re = 100$, $v_{max0} = 0.2$); (b) same, $v_{max0} = 0.4$.

$d_0 < 0$; a vortex with a counterclockwise circulation, when positioned at an initial $d_0 > 0$, increases the relative gas–droplet velocity in the vicinity of the droplet, and thus increases its convective heat transfer; by contrast, one with $d_0 < 0$ decreases the convective heating of the droplet.

An interesting case is that of $d_0 = 0$, where the droplet Nusselt number goes through a pattern of increase–decrease–increase, depending on the location of the advecting vortex [Fig. 2(a) and (b)]. When the vortex is upstream of the droplet, its counterclockwise circulation increases the convective effect, and thereby the droplet Nusselt number; very near the droplet, viscous interactions force it to pass 'underneath' the droplet [6] ('underneath' means in the lower half of the x, z symmetry plane in Fig. 1). In the droplet vicinity, the vortex reduces the convective effect of the base flow, and thus the droplet Nusselt number. When downstream of the droplet, the vortex once again strengthens the convective effect of the base flow, and so increases the droplet Nusselt number.

Nevertheless, when the vortex is initially positioned on the base flow symmetry axis ($d_0 = 0$), and therefore an increase in Nusselt number is followed by a

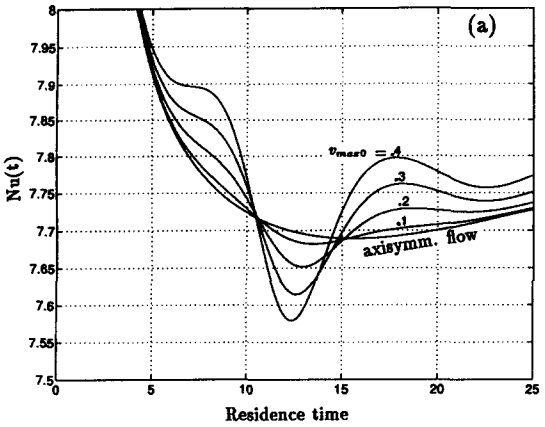

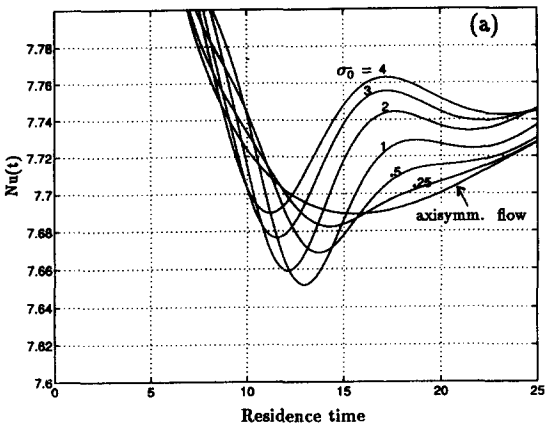

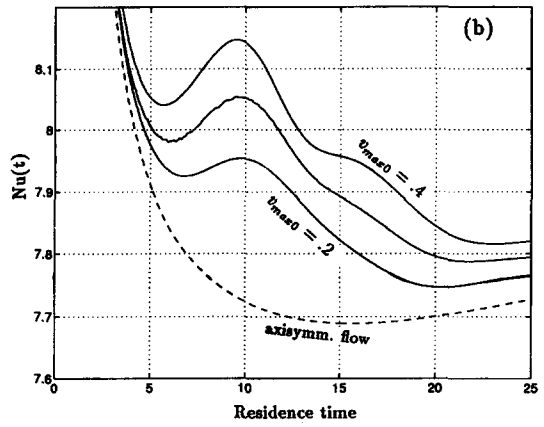

Fig. 3. Influence of the vortex initial tangential velocity (v_{max0}) on $Nu(t)$: (a) vortex advecting with $d_0 = 0$ ($Re = 100$, $\sigma_0 = 1$); (b) same, $d_0 = 1$.

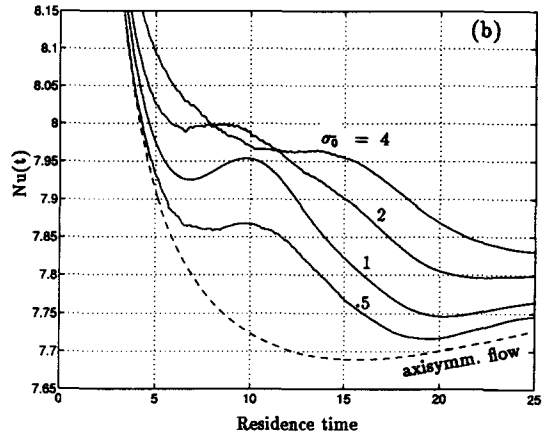

Fig. 4. Effect of the vortex initial radius (σ_0) on $Nu(t)$: (a) vortex advecting with $d_0 = 0$ ($Re = 100$, $v_{max0} = 0.2$); (b) same, $d_0 = 1$.

decrease, the summed variations yielding $\overline{Nu}$ are small; by contrast, the non-trivial changes in $\overline{Nu}$ occur when $d_0 \neq 0$.

3.2. *The effect of the vortex tangential velocity*

Figure 3(a) and (b) shows the influence of v_{max0} on the temporal Nusselt number when the vortex advects on [$d_0 = 0$, Fig. 3(a)] or off ($d_0 \neq 0$, Fig. 3(b)] the base flow symmetry axis; the corresponding pattern in an axisymmetric flow with the same Reynolds number has been also shown for comparison. Since $\Gamma_v \propto v_{max}$, vortices with larger v_{max} induce a stronger secondary flow in the uniform stream; thus, the droplet Nusselt number shows sensitivity to the vortex v_{max0}.

However, changes in $\overline{Nu}$ due to v_{max0} appear to be small for as long as $d_0 = 0$ [see Fig. 3(a), which indicates that $Nu(t)$ fluctuates around the axisymmetric curve for all values of v_{max0}]. This is the same as the previous observation that, as long as $d_0 = 0$, the vortex effect on $Nu(t)$ is sometimes augmenting and sometimes decreasing, yielding trivial changes from the axisymmetric value in $\overline{Nu}$. This was also seen when studying the effect of d_0. The observed negligible changes in $\overline{Nu}$ should not be interpreted as the insensitivity of the droplet heat transfer to the passage of the vortex or the vortex v_{max0}; simply stated, at $d_0 = 0$, cancellations are found in the averaging process. These cancellations are not encountered in computing $\overline{Nu}$ when $d_0 \neq 0$, such as the cases shown in Fig. 3(b); this more interesting effect of vortex tangential velocity that occurs when $d_0 \neq 0$ will be discussed later.

Data indicate that, overall, $\overline{Nu}/\overline{Nu}_{ax} - 1$ follows a linear dependence on v_{max0}.

3.3. *The effect of the vortex radius*

Figure 4(a) and (b) shows the influence of σ_0 on the temporal Nusselt number when the vortex advects on [$d_0 = 0$, Fig. 4(a)] or off [$d_0 \neq 0$, Fig. 4(b)] the base flow symmetry axis; the corresponding pattern in an axisymmetric flow with the same Reynolds number has been also shown for comparison.

Analogous to the previous observation, since $\Gamma_v \propto \sigma$, vortices with larger radii introduce stronger secondary flow in an otherwise uniform stream near the droplet; thus, the droplet Nusselt number appears sensitive to changes in the vortex radius. When the vortex advects on the base flow symmetry axis ($d_0 = 0$), in spite of the clear temporal sensitivity, the

time-averaged values of the Nusselt number compared to those in an axisymmetric flow (having the same Reynolds number) change by only 0.5% when $v_{max0} = 0.2$, and by about 1% when $v_{max0} = 0.4$, so that $\overline{Nu}/\overline{Nu_{ax}} = 1 \pm 1\%$. Similar to the case in the previous section, the trivial net change in the computed $\overline{Nu}$ in such cases is due to a combined effect of $d_0 = 0$ in the simulation and the nature of time-averaging of equation (8); it should not be interpreted as the insensitivity of the droplet convective heat transfer to the passage of the vortex or the vortex σ_0 [Fig. 4(a)].

Thus, when studying the effect of σ_0 on $\overline{Nu}$, larger values result when the vortex advects off the base flow symmetry axis [Fig. 4(b)]. Data indicate that $\overline{Nu}/\overline{Nu_{ax}} - 1$ follows a linear dependence on σ_0.

Figure 4(a) shows that, at early times, smaller radii yield larger $Nu(t)$, while, at later times, the results are reversed. This is because a vortex introduced upstream of the droplet with $d_0 = 0$ or small d_0/σ_0 has a 'head-on' collision with the droplet, and travels around its periphery before it advects downstream the droplet. If the vortex initial radius is small compared to the droplet radius, then, during the impact, the droplet is mostly outside the vortex inner core, and, therefore, the droplet heat transfer is augmented due to the vortex circulation; if the vortex initial radius is large, then the droplet is mostly within the vortex inner core and its solid-body-rotation velocity field; thus, the droplet near-field velocity is less strongly modified, resulting in a reduction in $Nu(t)$.

3.4. *The effect of the flow Reynolds number*

Figure 5(a) and (b) shows the influence of the base flow Reynolds number on the temporal Nusselt number when the vortex advects on [$d_0 = 0$, Fig. 5(a)] or off [$d_0 \neq 0$, Fig. 5(b)] the base flow symmetry axis; the corresponding pattern in an axisymmetric flow with the same Reynolds number has been also shown for comparison.

The higher the Reynolds number, the stronger the heat transfer fluctuations induced by the vortex, even though the strength of the vortex remains the same; thus, for example, a 30% fluctuations (i.e. $v_{max0} = 0.3$) in a uniform flow with $Re = 100$ has a stronger effect on the droplet Nusselt number than the same fluctuation does in a flow with $Re = 20$. The reason is simple: flows with lower Reynolds numbers are relatively more viscosity-dominated, and thus vortex-induced inertial changes are relatively more damped.

Analogous to the previous observations, when $d_0 = 0$ [Fig. 5(a)], there is barely a change in the time-averaged values of the Nusselt number due to a change in the base flow Reynolds number; $\overline{Nu}/\overline{Nu_{ax}} - 1$ changes over the range of Reynolds number by only 0.1% when $v_{max0} = 0.2$, and by 0.5% when $v_{max0} = 0.4$. Again, this is mostly the consequence of the choice $d_0 = 0$ and the nature of time-averaging in equation (8). Naturally, when $d_0 \neq 0$ [Fig. 5(b)], the computed changes in $\overline{Nu}/\overline{Nu_{ax}} - 1$ are stronger; such effects are

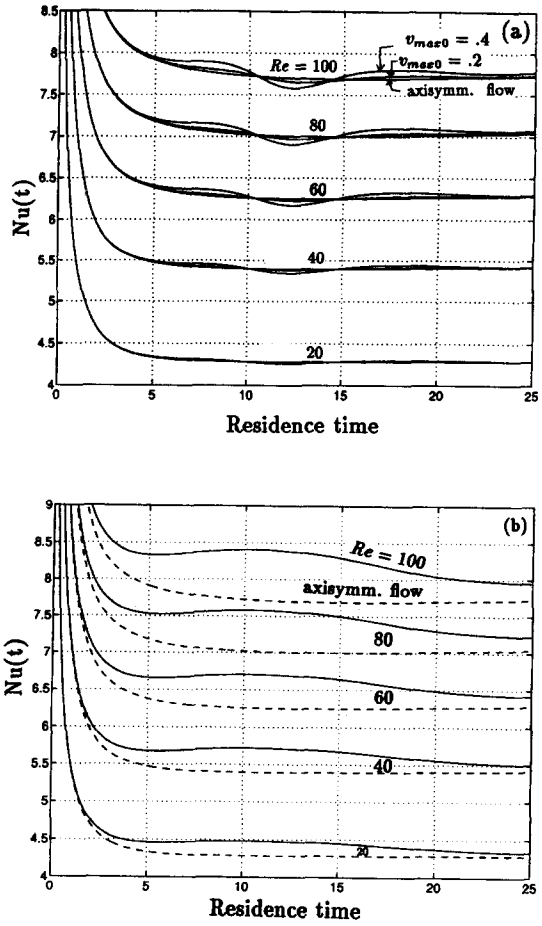

Fig. 5. Effect of the flow Reynolds number on $Nu(t)$: (a) vortex advecting with $d_0 = 0$ ($v_{max0} = 0.2$, 0.4, $\sigma_0 = 1$); (b) vortex advecting with $d_0 = +2$ ($v_{max0} = 0.3$, $\sigma_0 = 3$).

seen in Fig. 5(b) and will be discussed in the next section.

Data indicate that $\overline{Nu}/\overline{Nu_{ax}} - 1 \sim Re^{0.4}$; note that $\overline{Nu_{ax}} \sim Re^a$, where the exponent ranges from 0.427 to 0.573 (see the Appendix), so that approximately $\overline{Nu} - \overline{Nu_{ax}} \sim Re$. This implies that the time-averaged perturbations in Nusselt number have a stronger dependence on the Reynolds number than the Nusselt number itself does.

3.5. *Global self-similarity*

In the absence of the vortex, Nu and Nu_{ax} are identical, so that one may approximate the droplet Nusselt number using the correlation from Ref. [11] for a rigid sphere in an axisymmetric flow [4], or one may use the new correlation for axisymmetric flow past liquid spheres presented in the Appendix. With the vortex present in the domain, however, the axisymmetric flow correlation loses its applicability, and a new correlation accounting for the effect of the advecting vortex on the droplet heat transfer is to be used.

Such a correlation that accounts for the influence of the advecting vortex has been produced; all the data collapse into the functional form

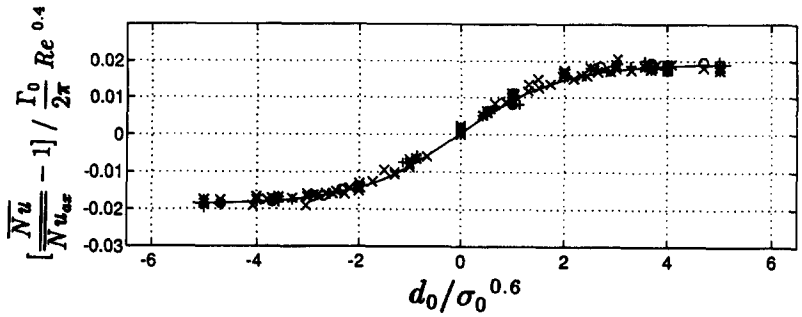

Fig. 6. Existence of self-similarity in time-averaged fluctuations in Nusselt number for a liquid droplet [equation (10)]: (●) markers (at $d_0/\sigma_0^{0.6} = 1$ and 4 each for $Re = 20$ and 100) represent results of simulations for a solid sphere.

$$\frac{\overline{Nu}}{\overline{Nu}_{ax}} = 1 + 0.019 \frac{\Gamma_0}{2\pi} Re^{0.40} \tanh\left(0.50 \frac{d_0}{\sigma_0^{0.6}}\right) \tag{10}$$

within the range of the parameter study: $20 \leqslant Re \leqslant 100$; $0.25 \leqslant \sigma_0 \leqslant 4$; $0.1 \leqslant v_{max0} \leqslant 0.4$; $-5 \leqslant d_0 \leqslant 5$. This covers a range of vortex circulation varying by nearly two order-of-magnitudes: $\Gamma_0 \in (0.16, 10.05)$. All the simulations are for a cold n-octane droplet in hot air, and so $Pr_l = 8.527$, and $Pr_g = 0.739$. The correlation coefficient for the above fit is $r = 0.956$; ($r \equiv 1 - [\Sigma_{i=1}^{n} (y_{\text{actual}_i}/y_{\text{fit}_i} - 1)^2]^{0.5}$; $y = \overline{Nu}/\overline{Nu}_{ax}$). A plot of this correlation and its comparision with the present data is shown in Fig. 6. For $|d_0/\sigma_0^{0.6}| \to 5$, $\overline{Nu}/\overline{Nu}_{ax} - 1$ approaches an asymptote; here, profiles of $Nu(t)$ are still at least modestly different, apparent in Fig. 2. For $d_0 = 0$, the data yield $\overline{Nu}/\overline{Nu}_{ax} - 1 \sim 0.001$, which is negligible in practical terms.

The correlation of equation (10) indicates that a change in the sign of either d_0 or circulation produces a change in the sign of the deviation of the averaged Nusselt number from the averaged base axisymmetric value. Note that this correlation holds for bounded values of the fluctuating velocity; in particular, the vortex is not strong enough to reverse the free-stream flow direction ($v'_{max0}/U'_\infty < 1$).

While the droplet internal circulation is instrumental in its internal temperature distribution, it is, however, well known that, due to the large density ratio between the liquid and the gas phase, the internal circulation is nevertheless weak, and thus the interface velocity remains negligible compared to the free-stream gas velocity. Therefore, the structure of the viscous and thermal layers on the gas side of the interface are not substantially changed. Only minor changes in Nusselt number for the gas-phase boundary layer result. (However, internal circulation cannot be neglected because it will still have a significant effect on the interface temperature, and, therefore, on the heat transfer through the gas-phase boundary layer.) This allows approximating the Nusselt number for a cold droplet in a hot gas from correlations or simulations sought for a rigid sphere, and vice versa. It has been further verified in this investigation that simulations for a solid sphere in the presence of an advecting vortex yielded $\overline{Nu}$ values close to those for a liquid sphere, fitting equation (10), and thus confirming that this correlation could be used for a solid sphere in comparable condition, as well. This is also shown in Fig. 6.

Depending on the asymptotic value of $d_0/\sigma_0^{0.6}$, equation (10) may be recast into two simpler forms. For small values of $d_0/\sigma_0^{0.6}$, tanh is approximately linear in its argument ($\tanh x \to x$ as $x \to 0$); rearranging variables and using $\overline{Nu}_{ax} \sim Re^{0.573}$ yields

$$\overline{Nu} - \overline{Nu}_{ax} \sim \pm \sigma_0^{0.4} Re^{-0.027} Re_{v_{d_0}}. \tag{11}$$

Conversely, for large $d_0/\sigma_0^{0.6}$ (and using $\tanh x \to 1$ as $x \to \infty$), equation (10) may be again rearranged to give

$$\overline{Nu} - \overline{Nu}_{ax} \sim \pm Re^{-0.027} Re_{v_{\sigma_0}} \tag{12}$$

where $Re_{v_{d_0}}$ and $Re_{v_{\sigma_0}}$ are Reynolds numbers defined solely based on the vortex characteristics: $Re_{v_{d_0}} = v'_{max0} d'_0/\nu'$ and $Re_{v_{\sigma_0}} = v'_{max0}\sigma'_0/\nu'$, with the characteristic length in the former being the vortex offset distance from the base flow symmetry axis and in the latter the vortex core size. The + sign in equations (11) and (12) applies for positive d_0 and counter-clockwise vortex rotation, or for negative d_0 and clockwise rotation. Otherwise, a negative sign appears.

A few observations are made here. For small $d_0/\sigma_0^{0.6}$ [equation (11)], the perturbations in the Nusselt number induced by the vortex explicitly depend on the vortex core size σ_0; a plausible explanation is that in this range the vortex embraces the droplet partly or fully during the interaction, and thus its core size is of significance. By contrast, for large $d_0/\sigma_0^{0.6}$ [equation (12)], the droplet remains totally outside the vortex core, and thus it is the vortex-induced inertia embedded in its circulation $\Gamma_{v_0} \sim v'_{max0}\sigma'_0$ or equivalently in $Re_{v_{\sigma_0}}$ that matters in the perturbations. It is noteworthy that for both asymptotes the primary dependence of perturbations appears to be on Re_v and not Re; i.e. they appear to have only a weak dependence on Re.

All of the efforts, however, to produce a simple correlation for the rms values of the Nusselt number, Nu_{rms}, such as one qualitatively similar to the one above for $\overline{Nu}$, remained fruitless. Instead, some comments and insight on the dependence of Nu_{rms} on all of the four parameters involved are presented.

Figure 7(a) shows Nu_{rms} changing as a function of d_0; it is obvious that Nu_{rms} peaks at $|d_0| = 2$ (an observation nearly identical to that made from $\overline{Nu}$ values); however, it is not symmetric with respect to $d_0 = 0$ (unlike $\overline{Nu}$ values), but demonstrates relatively larger values for $d_0 < 0$; this occurs since, for $d_0 < 0$, $Nu(t)$ values exhibit a relatively larger initial drop [Fig. 2(a) and (b)], yielding larger Nu_{rms} values. [Sample calculations, with data within $t \in (0, t_1)$ excluded with $t_1 \gg 2$ (see Section 2), confirmed this: Nu_{rms} values appeared symmetric with respect to $d_0 = 0$.]

Figure 7(b-1) and (b-2) shows changes in Nu_{rms} due to σ_0. In contrast to observations made from the time-averaged values of Nusselt number, and owing to the nature of computing an rms value in which the variations are squared and so no cancellation takes place [equation (9)], Nu_{rms} values with $d_0 = 0$ could be larger than those with $d_0 > 0$ [Fig. 7(b-2)].

The influence of the Reynolds number on the rms values is shown in Fig. 7(c-1) and (c-2); they exhibit a non-linear dependence on Re, irrespective of the choice of the initial value for the remaining three parameters (σ_0, d_0, v_{max0}).

4. CONCLUSIONS

The unsteady interaction between a cylindrical vortex tube and a liquid droplet in a uniform flow has been investigated by pursuing a study of each of the four parameters affecting the strength of this inter-

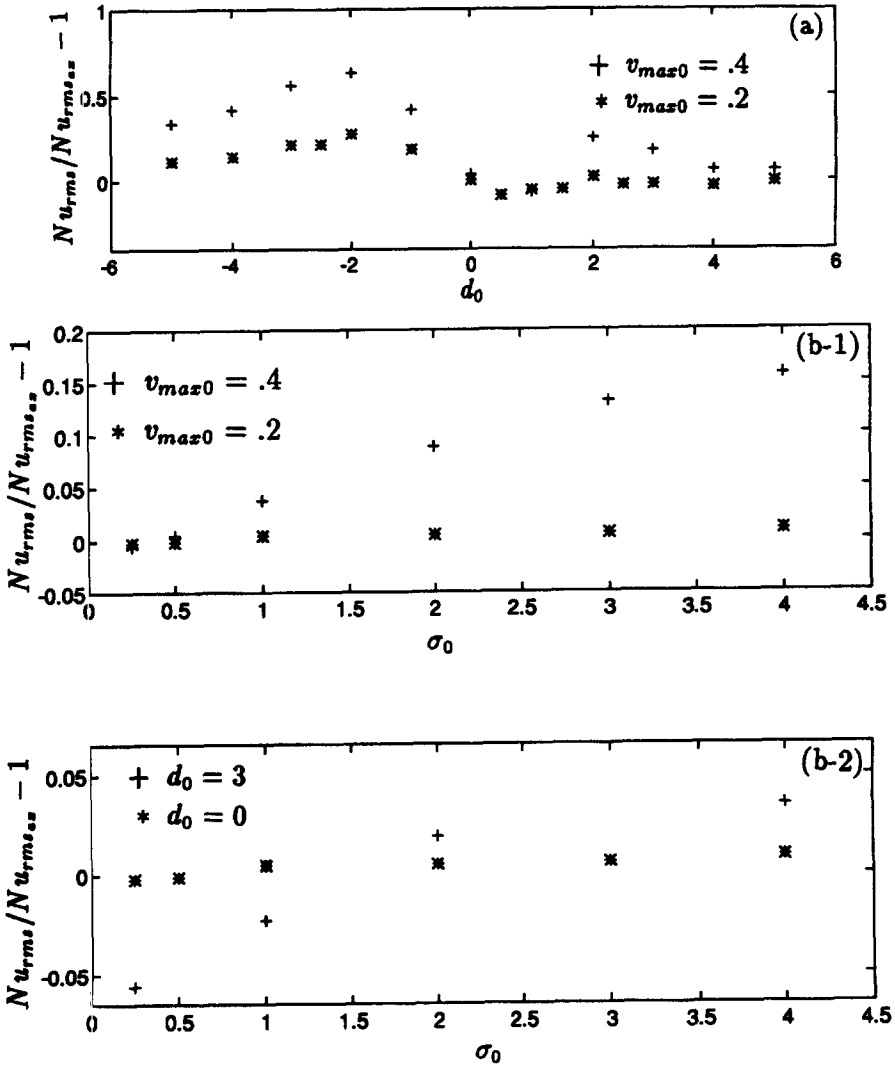

Fig. 7. Root-mean-squared Nusselt number (Nu_{rms}) changing due to: (a) vortex initial distance d_0; ($\sigma_0 = 1$, $Re = 100$); (b) vortex initial radius σ_0 with $d_0 = 0$ (b-1: $Re = 100$) and varying d_0 (b-2: $Re = 100$, $v_{max0} = 0.2$); (c) Reynolds number Re with $d_0 = 0$ (c-1: $\sigma_0 = 1$) and varying d_0 (c-2: $\sigma_0 = 1$, $v_{max0} = 0.4$).

(*Continued overleaf.*)

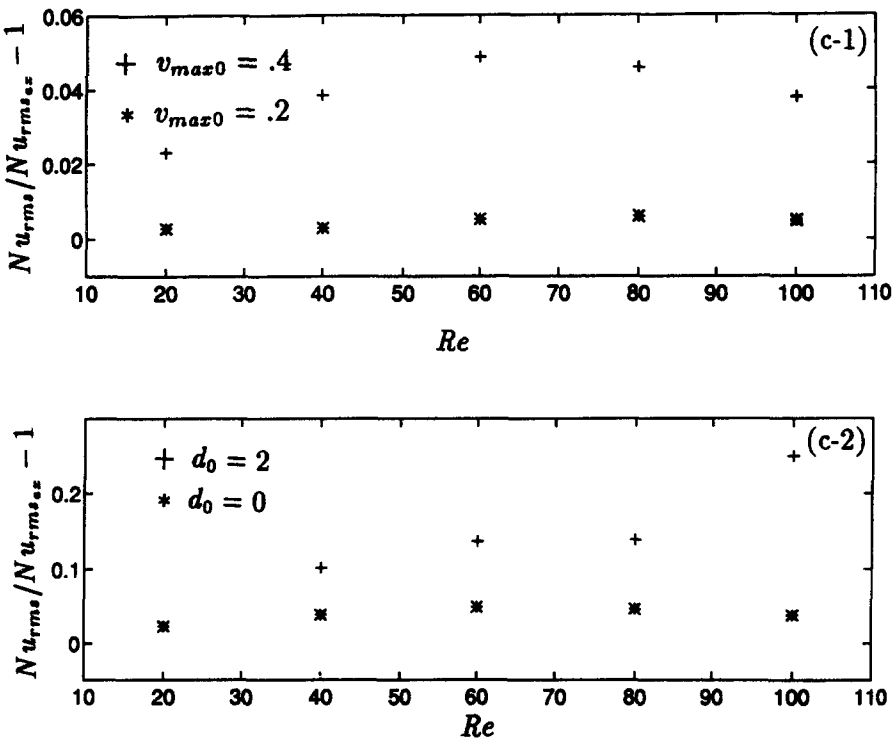

Fig. 7—*Continued.*

action and modifying the droplet Nusselt number. Particular attention has been paid to the effect of these parameters on the transient and time-averaged values of the droplet Nusselt number. A correlation quantifying the effect of the advecting vortex on the droplet heating has been produced, signifying a self-similar behavior for the average effect in this unsteady problem. The reported correlation compliments the existing ones for droplet heating in axisymmetric flows that occur in the absence of an advecting vortex [11]. It may also be used for a rigid sphere in comparable conditions in the presence of an advecting vortex.

When the vortex advects towards and then past the droplet starting upstream 'on' the symmetry axis of the base flow, the droplet Nusselt number first increases and then decreases; thus, the time-averaged Nusselt number is nearly equivalent to that in an axisymmetric flow, even when the vortex simulates up to 40% fluctuation in the base flow. Conversely, when the vortex advects 'off' the base flow symmetry axis, the time-averaged Nusselt number is changed due to the vortex-induced fluctuations. Whether this has an augmenting or inhibiting effect on the droplet heating (compared to one in an axisymmetric flow) depends on two factors: the vortex circulation orientation and also whether it advects 'above' or 'below' the symmetry axis in the plane of symmetry (Fig. 1). The time-averaged Nusselt number is linearly proportional to the vortex circulation; also, it follows $\sim\tanh(0.5d_0/\sigma_0^{0.6})$, and thus has an exponential dependence on the vortex initial position d_0. Furthermore, due to this exponential dependence, the influence of the vortex on the time-averaged Nusselt number reaches an asymptote for relatively larger d_0. The computations here are limited to $|d_0| \leqslant 5$. Naturally, one expects that when the vortex advects 'very' far from the droplet, it will have no or a negligible effect on the droplet heating.

The hyperbolic tangent correlation also yields two interesting limits. For small $d_0/\sigma_0^{0.6}$ and large Re, $\overline{Nu} - \overline{Nu}_{ax}$ is linearly proportional to a Reynolds number based on d_0 and the vortex maximum tangential velocity, as well as having a dependence on the vortex core size [equation (11)]. For large $d_0/\sigma_0^{0.6}$ and large Re, $\overline{Nu} - \overline{Nu}_{ax}$ is linearly proportional to a Reynolds number based on the vortex core size and its maximum tangential velocity, as shown in equation (12). Moreover, and interestingly enough, in both limits it is the advecting vortex that appears to influence the Nusselt number perturbations and not the base flow, since there appears to exist only a weak dependence on the base flow Reynolds number.

It is emphasized that, in parallel studies investigating changes in fluid dynamic properties of solid spheres (lift and moment coefficients) [6], a similar dependence of fluctuations in fluid dynamic properties on vortex parameters has been observed. Specifically, the induced fluctuations appeared to depend on the vortex circulation in a similar fashion. A marked dependence of the Nusselt number fluctuations on the fluid dynamics variations explains the similarity between the conclusions of the two studies.

In the absence of vortical structures, $\overline{Nu}_{ax} \sim O(Re^{0.573})$, thus prompting one to anticipate its perturbations, $\overline{Nu}-\overline{Nu}_{ax} \sim O(Re^{0.573})$, as well. However, this is *not* the case; instead, the induced perturbations follow $\overline{Nu}-\overline{Nu}_{ax} \sim O(Re^{0.973})$.

These calculations have not considered the effect of the deflection of the droplet due to the fluctuating velocity. Nor has the combined effects of an array of vortical structures been considered. These important issues should be addressed in the future.

Based on the present findings, it is may be speculated that, in a spray combustion system, the vortex–droplet interactions within the Kolmogorov scale can have significant effects on the droplet convective heat transfer.

Acknowledgements—This work has been supported by the Air Force Office of Scientific Research under grant No. F49620-93-1-0028, with Dr Julian Tishkoff acting as the technical monitor. The authors thank Professor S. Elghobashi for his comments on the self-similar correlation. The support of the University of California, Irvine, Office of Academic Computing through the use of their Convex C3840, and the help of Mr Donald Frederick and Dr Allen Schiano, are gratefully appreciated. San Diego Supercomputing Center also generously supported this work through their supercomputer time allocation.

REFERENCES

1. Sirignano, W. A., Fluid dynamics of sprays—1992 Freeman Scholar Lecture. *Journal of Fluids Engineering*, **115**, 345–378.
2. Tong, A. Y. and Sirignano, W. A., Oscillating vaporization of fuel droplets in an unstable combustor. *Journal of Propulsion and Power*, 1989, **5**, 257–261.
3. Duvuur, A., Chiang, C. H. and Sirignano, W. A., Oscillating fuel droplet vaporization: driving mechanism for combustion instability. *Journal of Propulsion and Power*, 1996, **12**, 358–365.
4. Abramzon, B. and Sirignano, W. A., Droplet vaporization model for spray combustion calculations. *International Journal of Heat and Mass Transfer*, 1989, **32**, 1605–1618.
5. Chorin, A. J., *Vorticity and Turbulence*. Springer-Verlag, Berlin, 1994.
6. Kim, I., Elghobashi, S. and Sirignano, W. A., Unsteady flow interactions between an advected cylindrical vortex tube and a spherical particle. *Journal of Fluid Mechanics*, 1995, **288**, 123–155.
7. Kim, I., Elghobashi, S. and Sirignano, W. A., Unsteady flow interactions between a pair of advected cylindrical vortex tubes and a rigid sphere. *International Journal of Multiphase Flow*, 1997, **23**, 1–23.
8. Kim, I., Elghobashi, S. and Sirignano, W. A., Three-dimensional flow over two spheres placed side by side. *Journal of Fluid Mechanics*, 1993, **246**, 465–488.
9. Saffman, P. G., *Vortex Dynamics*. Cambridge University Press, Cambridge, 1992.
10. Spalart, P. R., Numerical simulation of separated flows. PhD dissertation, Stanford University, Stanford, CA, 1982.
11. Clift, R., Grace, J. R. and Weber, M. E., *Bubbles, Drops, and Particles*. Academic Press, New York, 1978.

APPENDIX

In an axisymmetric flow, and following the assumption that the effect of the droplet internal circulation on the droplet heating is small, one may use the Nusselt number correlation from Ref. [11] for a rigid sphere:

$$Nu = 1+(1+Pr\,Re)^{1/3}\,Re^{0.077} \quad Re \leqslant 400. \qquad \text{(A1)}$$

This correlation has been recommended for spray combustion computations [4]. For particles having $Re \geqslant 10$ in media with $Pr \approx 1$, this suggests $Nu-1 \sim Re^{0.410}$.

This suggested correlation has been modified by accounting for the droplet internal circulation. The calculations (non-vaporizing *n*-octane droplet in air, $10 \leqslant Re \leqslant 100$) suggest a fit of the form

$$Nu-1 = 0.927Re^{0.427} \quad 10 \leqslant Re \leqslant 100. \qquad \text{(A2)}$$

The authors note, however, that this form is somewhat clumsy since one should expect $Nu = 2$ at $Re = 0$. A preferred fit therefore is

$$Nu-2 = 0.412Re^{0.573} \quad 10 \leqslant Re \leqslant 100. \qquad \text{(A3)}$$

Equations (A2) and (A3) have correlation coefficients of 0.97 and 0.99, respectively.

It is suggested that the slight increase in the exponent of Re [compared to the exponent 0.40 resulting from equation (A1)] is a contribution of the droplet internal circulation. That is, the boundary layer and thermal layer thicknesses are decreased slightly due to the motion along the interface. This results in an increase in heat transfer rate from the hot ambient gas to the cold droplet.

Finally, the accuracy of the above equations is compared. Equations (A2) and (A3) were produced with simulations using (21,21,21) and (15,21,21) mesh points in (r, θ, ϕ) coordinates in the gas and liquid phases, respectively, and yield Nu values nearly identical to those of equations (A1) for $Re = 10$, but about 13% larger near $Re = 100$. A simulation using (41,41,41) and (15,41,41) mesh points in gas and liquid phases for $Re = 100$ produced a value that was still 5% above that given by equation (A1). This discrepancy was expected since equation (A1) is suggested by Ref. [11] for a rigid sphere where the absence of internal circulation yields Nu values lower than those of a liquid sphere.